Dynamics of Atmospheres and Oceans 75 (2016) 91–101

Contents lists available at ScienceDirect

Dynamics of Atmospheres and Oceans

journal homepage: www.elsevier.com/locate/dynatmoce

The 10–30-day intraseasonal variation of the East Asian winter monsoon: The temperature mode

Suxiang Yao [a], Qingfei Sun [a], Qian Huang [a,b,*], Peng Chu [c]

[a] CDRC/ESMC, International Laboratory on Climate and Environment Change, Key Laboratory of Meteorological Disaster of Ministry of Education, Nanjing University of Information Science and Technology, 219 Ningliu Road, Nanjing, 210044, China
[b] Collaborative Innovation Center on Forecast and Evaluation of Meteorological Disasters, 219 Ningliu Road, Nanjing, 210044, China
[c] Jiangsu Sub-bureau of East China Regional Air Traffic Management Bureau, CAAC, Nanjing, 211113, China

ARTICLE INFO

Article history:
Received 1 July 2016
Received in revised form 13 July 2016
Accepted 16 July 2016
Available online 18 July 2016

Keywords:
East Asian winter monsoon (EAWM)
Intraseasonal oscillation (ISO)
Air temperature
Arctic oscillation
Plateau

ABSTRACT

East Asia is known for its monsoon characteristics, but little research has been performed on the intraseasonal time scale of the East Asian winter monsoon (EAWM). In this paper, the extended reanalysis (ERA)-Interim sub-daily data are used to study the surface air temperature intraseasonal oscillation (ISO) of the EAWM. The results show that the air temperature (2-m level) of the EAWM has a dominant period of 10–30 days. Lake Baikal and south China are the centers of the air temperature ISO. An anomalous low frequency (10–30-day filtered) anticyclone corresponds to the intraseasonal cold air. The 10–30-day filtered cold air spreads from Novaya Zemlya to Lake Baikal and even to South China. The ISO of the Arctic Oscillation (AO) index influences the temperature of the EAWM by stimulating Rossby waves in middle latitude, causing meridional circulation, and eventually leads to the temperature ISO of the EAWM. RegCM4 has good performance for the simulation of the air temperature ISO. The simulated results indicate that the plateau is responsible for the southward propagation of the intraseasonal anticyclone. The anticyclone could not reach South China when there was no plateau in western China and its upper reaches.

1. Introduction

Since the intraseasonal oscillation was first found in the tropical atmosphere in the early 1970s (Madden and Julian, 1971, 1972), many studies have been conducted to study the characteristics and the mechanism of the ISO, and the results include its seasonal-dependent propagation (Madden and Julian 1994; Maloney 2009; Hsu and Li 2012), the Rossby-Kelvin wave couplet structure in the horizontal distribution (Hendon and Salby, 1994; Kiladis and Wheeler, 1995; Chatterjee and Goswami, 2004), the tilting vertical moisture and wind profile (Sperber, 2003; Jiang et al., 2004), and the interannual variations of the ISO in tropical regions (Slingo et al., 1999; Lin and Li, 2008; Li, 2014).

There are some obvious differences in the ISO between the tropical and the extratropical areas. The extratropical ISO was discovered in the 1980s (Anderson and Rosen, 1983; Krishnamurti and Gadgil, 1985) and is independent of tropical forcing (Knutson and Weickmann, 1987; Ghil and Mo, 1991). For the boreal summer season, the East Asian monsoon rainfall in the extratropical regions presents both 20–50-day oscillation and 10–20-day oscillation (Yang et al., 2010; Mao and Chan,

* Corresponding author at: 1001# Building of Meteorology, No. 219, Ningliu Road, Nanjing University of Information Science & Technology, Nanjing, Jiangsu, (Postcode: 210044) China.
E-mail address: huangq@nuist.edu.cn (Q. Huang).

http://dx.doi.org/10.1016/j.dynatmoce.2016.07.001

2005; Zhu and Li, 2016). The zonal shift of the South Asian High at 200 hPa displays a dominant periodicity of 10–50 days, and is closely related to the southward movement of intraseasonal perturbations originating in middle latitudes (Yang and Li, 2016a,b). Shao et al. (2011) investigated the circulation background and meteorological factors of the extreme freeze in southern China during the winter of 2007/2008 and found that the 10–20-day oscillation is an important mode for the atmospheric changes during periods of sustained freezing rainfall and snow. For the high latitude regions, the winter ISO in Eurasia mainly shows the 10–30-day oscillation and propagates southeastward (Yang and Li, 2016a,b). In the mid-high latitudes of the north Pacific, the geopotential height ISO propagates westward. Wang et al. (2012, 2013) found that the mid-latitude ISO in the north Pacific is primarily caused by local physical processes.

East Asia is known for its monsoon climate. The spate of persistent freezing rain and snow in recent years could be a statistical quirk. For example, in January and February of 2008, South China experienced four severe cold rain and snow events; the super cold wave in January 2016 broke the lowest temperature record in East Asia for the last 50 years, and because of its long period process and wide range of influence, the extreme cold weather always leads to huge economic losses. A recent study showed that the persistent meteorological disasters belong to medium- and long-term weather processes and often have ISO characteristics. The disasters appear during the active phase of the ISO (Ma et al., 2011; Hsu et al., 2015). It is worth noting that previous studies have not considered the ISO of the EAWM. Motivated by the research needs, we investigated the ISO of the surface temperature of the EAWM in this paper.

The remaining part of this paper is organized as follows. Section 2 describes the data and methods used in this study. The study results, including the air temperature distribution and evolution on an intraseasonal time scale are presented in Section 3. The relationship between the temperature ISO and Arctic Oscillation is analyzed in Section 4. Section 5 discusses the plateaus influences on the temperature ISO. The conclusions and discussions are given in Section 6.

2. Dataset and methods

2.1. Data

The data used in this paper consist of ERA-Interim 6 h reanalysis data of the temperature at 2 m, the geopotential height, and meridional wind and zonal wind at pressure levels with a horizontal resolution of $0.5^\circ \times 0.5^\circ$ (Dee et al., 2011), and the daily data are the average of the 6-hourly data. In addition, the daily AO index data are downloaded from the website: http://www.cpc.ncep.noaa.gov/products/precip/CWlink/daily_ao_index/ao.shtml. The AO index has been used for research in many fields (Higgins et al., 2002; Higgins et al., 2000; Zhou et al., 2001).

2.2. Method

The seasonal cycle is firstly removed from the raw data. Power spectrum-analysis is used to analyze the dominant period of the air temperature. The Butterworth band-pass (10–30-day filtered) filter (Hamming 1977) is chosen to derive the intraseasonal signals. Regression analysis is used to obtain the circulation characteristics of the intraseasonal temperature anomalies. Winter is defined as the time period from November 1 to April 30. The total number of days of the 34 winters (from 1979/1980 to 2012/2013) is 6163.

2.3. Experiment design

Developed by the International Center for Theoretical Physics of Italy, the Regional Climate Model RegCM is a powerful tool to study climate change (Dickinson et al., 1989; Giorgi and Mearns, 1999; Pal et al., 2007). In this paper, the latest version, RegCM4 (Gao et al., 2013), is used to simulate the winter intraseasonal temperature and its relationship with the plateaus, including the Tibetan and Mongolian plateau.

In the model, the planetary boundary layer scheme developed by Holtslag and Emanuel is chosen as the convective precipitation scheme. The system uses the radiation method of the National Center for Atmospheric Research (NCAR) Coupled Climate Model, version 3 (CCM3). In the ocean surface, the Zeng scheme is chosen for ocean flux. The horizontal resolution of the model is 60 km. A ten-year simulation is performed from 1999 to 2008, and there are 9 winters (from 1999/2000 to 2007/2008, 1632 days). The two experiments include a control run (CTR) and the no-plateau run (NOP). The difference between the CTR run and the NOP run is the topography. In the control run, we use the actual terrain, and in the no-plateau run, the altitude is set to zero.

3. The characteristics of the 10–30-day intraseasonal temperature

The 34 winter average surface air temperature and sea level pressure (SLP) is shown in Fig. 1. The surface system of the EAWM includes the Mongolian high and the Aleutian low (Fig. 1, contoured). Generally, there is a northerly wind between the Mongolian high and Aleutian low, as shown in the green box of Fig. 1. The strength of the north wind is determined by the air pressure differences between the anticyclone and the cyclone. The temperature distribution shows cold continents and the warm oceans in winter. In Eurasia, it is cold in the north and warm in the south. The following study focuses on the region in the green box, which is the eastern Asian monsoon region (0–60°N 100–140°E). In the middle troposphere,

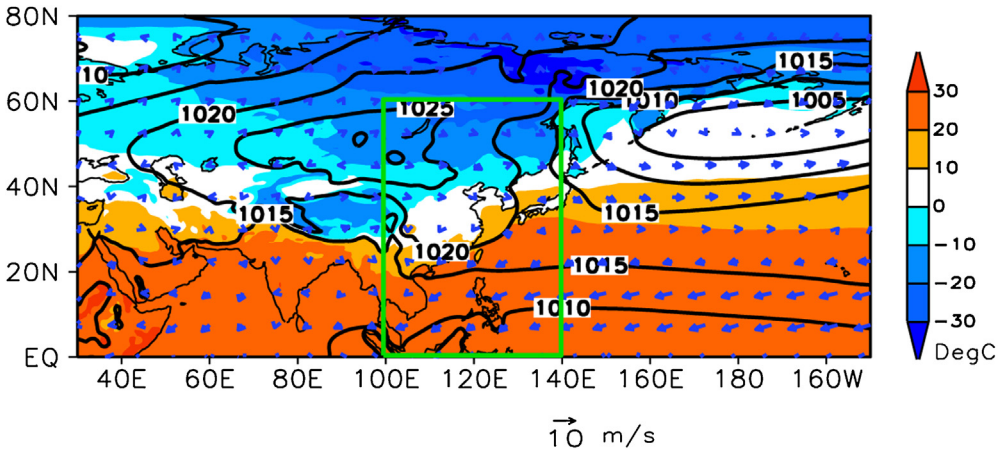

Fig. 1. The winter average (from 1979/1980 to 2012/2013) air temperature at 2 m (color shaded, unit: °C), SLP (contour, unit: hPa) and wind at 10 m (vector, unit: m s^{-1}). (For interpretation of the references to colour in this figure legend, the reader is referred to the web version of this article.)

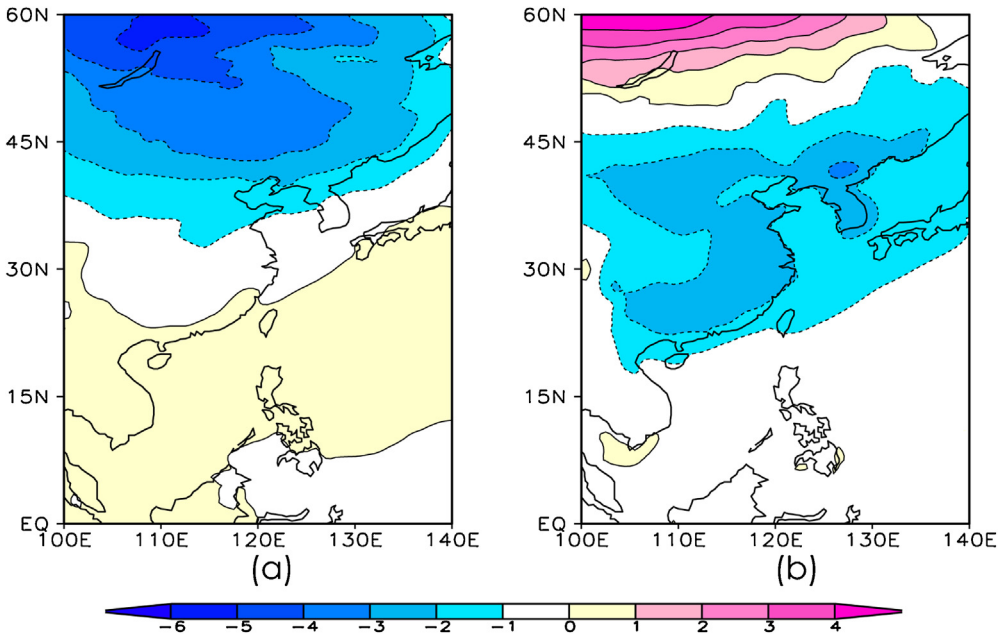

Fig. 2. The first EOF mode (EOF1, a) and second EOF mode (EOF2, b) of the air temperature at 2 m of the EAWM.

the wind is westerly in the mid-high latitude; and there is an eastern Asian trough in front of the monsoon region (figure omitted).

To study the temporal and spatial variation of the daily air temperature, the empirical orthogonal function (EOF) decomposition is used to obtain the primary mode of the air temperature at 2 m high, and the results show that the variance contribution of first two modes is 50%, and it is 32% for the first EOF mode (EOF1) and 18% for the second EOF mode (EOF2). EOF1 (Fig. 2a) gives the antiphase between the land and the ocean, with a strong center in Lake Baikal and a weak belt in the ocean. If the time series of EOF1 is positive, then it is cold in Lake Baikal. The two temperature anomaly centers of EOF2 (Fig. 2b) are located on land, and the temperature in the Lake Baikal is in contrast to that in China. If the time series of EOF2 is positive, then it is cold in China and warm in the Lake Baikal (Fig. 2).

The EOF decomposition also shows the time evolution of the distribution modes. To determine the dominant period of the air temperature activity, the time series of the air temperature EOF1 (the first principal component, PC1) and PC2 (the second principal component) are subjected to a power spectrum analysis. The results indicate that the statistically significant signal of both PC1 and PC2 appears at a period of 10–30 days (Fig. 3), especially 10–20 days. Considering these factors, in the following study, the intraseasonal oscillation period is 10–30 days, unless indicated otherwise.

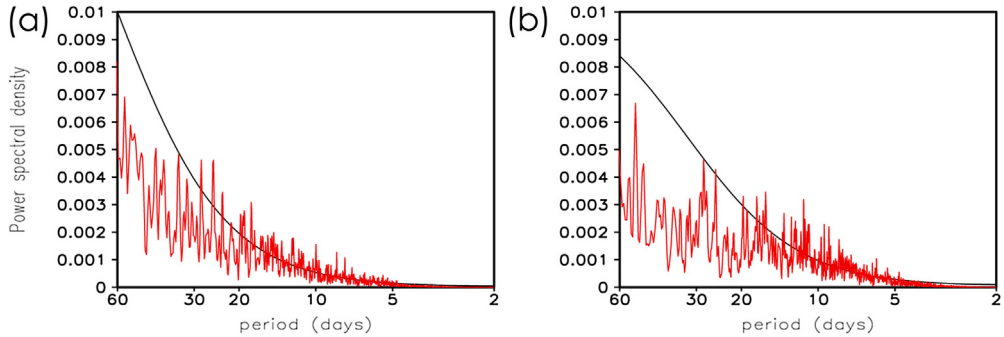

Fig. 3. Power spectral analysis of the time series of EOF1 (a) and EOF2 (b); the red and black lines denote the spectrum density and the 0.01 significance level of the red noise, respectively. (For interpretation of the references to colour in this figure legend, the reader is referred to the web version of this article.)

3.1. Propagation of the air temperature ISO

The EOF decomposition of the 10–30-day filtered air temperature has almost the same distribution as the raw data (Fig. 4a,b). The variance contribution of first two modes is 54%, which is larger than that of the raw data. The variation contribution is 32% for the first EOF mode and 22% for the second EOF mode. There is a slight difference in the EOF2 distribution between the raw data and the intraseasonal temperature. An oscillation center appears in South China on an intraseasonal time scale (Fig. 4b). The time lead-lag correlation coefficients between the first two principal components (PC1 and PC2) are depicted in Fig. 4c. The results show that PC1 leads PC2 by 4 days because of the significant positive correlation (0.59), and the two leading modes of EOF reflect the same propagating mode at different phases.

We select PC1 for further analysis and define the ISO event as a peak value larger than 1.5 standard deviations. During the 34 winters, there are 128 ISO events for PC1. The peak day is named 'day 0', one day before the peak day is named as 'day −1', and one day after the peak day is named 'day 1'. The evolution of the composite 10–30 day filtered air temperature anomalies from day −10 to day 10, at an interval of 2 days, is portrayed in Fig. 5. Day 0 represents the time when the center of the intraseasonal temperature anomalies appears at the same location as shown in the EOF1 structure (Fig. 4a), including the cold center in Lake Baikal and the warm center at high latitude. The cold center of the intraseasonal temperature at day 4 is in China, which is similar with the structure of EOF2 (Fig. 4b). Ten days before the peak day, the cold (negative) center is locates at Novaya Zemlya at high latitude, and Lake Baikal is warm. Day-by-day, the cold air spreads southeastward from Novaya Zemlya to Eurasia and even to South China. The strength of the intraseasonal cold air is strong over land. When it spreads to the sea-land interface, the strength of the intraseasonal cold air decreases. The significant centers of the intraseasonal temperature mostly appear on land, especially in eastern Asia. The intraseasonal cold center is in front of the low frequency anticyclone, and the warm center is in front of the low-frequency cyclone. From day −10 to day 10, a low-frequency anticyclone moves from the Arctic ocean to South China and then to the Pacific. The strength of the low-frequency anticyclone and the intraseasonal cold center increases when it moves to Lake Baikal.

3.2. Circulation of the air temperature ISO

Circulation has important influence on the air temperature. Regression analysis is used to study the corresponding circulation of the different intraseasonal air temperature modes. Based on PC1 and PC2 of the 10–30-day filtered temperature EOF analysis, the regression results of the temperature show the same distribution as EOF1 and EOF2. For PC1 (Fig. 6a,c), an anomalous low-frequency (10–30-day filtered) high appears in the surface of Lake Baikal (Fig. 6a), which is between the positive and the negative geopotential height centers at 500 hPa. In the cold center, there is a north wind anomaly in the low troposphere (850 hPa) (Fig. 6c). For PC2 (Fig. 6b,d), the cold center moves to China, even to South China. Over Eurasia, an anomalous low-frequency cyclone appears in the north of Lake Baikal, and an anomalous low-frequency anticyclone moves to China (Fig. 6b). The north wind is very strong in eastern China, even spreading to the South China Sea (Fig. 6d). The geopotential height in Lake Baikal is positive, and the east coast of East Asia has negative geopotential height on the intraseasonal scale at 500 hPa.

4. AO and the temperature ISO of the EAWM

The intraseasonal temperature mode of the EAWM is closely related to the atmospheric circulation anomaly at high and middle latitude. Fig. 5 shows the intraseasonal temperature center moving from the Arctic to eastern Asia. The Arctic air that penetrates the middle latitudes is related to the Arctic Oscillation (AO). The AO index is the dominant pattern of SLP variation north of 20°N latitude, and it is characterized by pressure anomalies of one sign in the Arctic, with the opposite anomalies centered at approximately 37–45°N (Thompson and Wallace, 1998). Recent study also shows that there exists

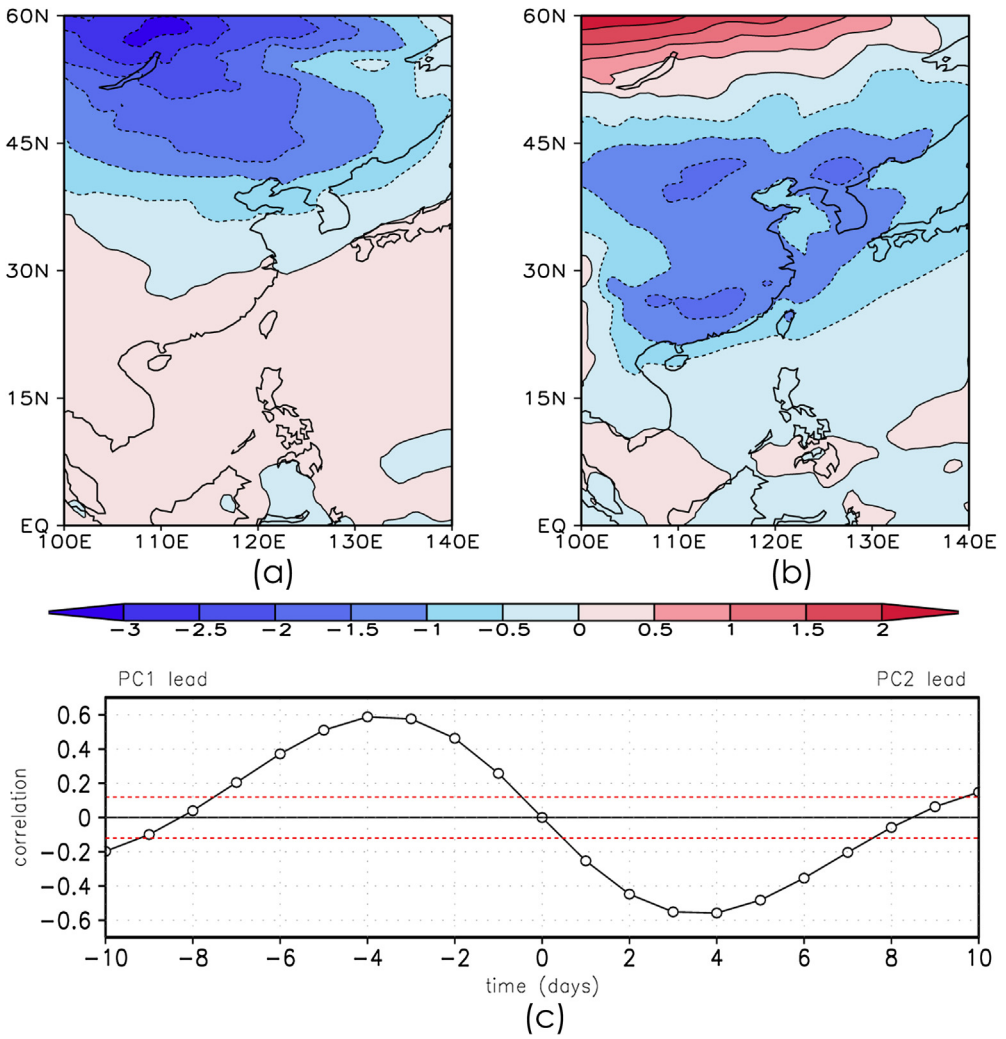

Fig. 4. The first EOF mode (EOF1, a) and the second EOF mode (EOF2, b) of the 10–30-day filtered air temperature at 2 m of the EAWM; (c): The lead-lag correlation coefficients between PC1 and PC2. The red dashed lines denote the 0.001 significance level. (For interpretation of the references to colour in this figure legend, the reader is referred to the web version of this article.)

a polar-tropical seesaw mode that characterizes with the out of phase fluctuations of SLP between the polar and tropical regions in boreal winter (Tang and Guan, 2015). We further analyze the relationship between AO and the temperature of the EAWM on the intraseasonal time scale.

The lead-lag correlation between the intraseasonal AO index and the air temperature at 2 m is shown in Fig. 7. Here, PC1 and PC2 are the time series of the intraseasonal temperature EOF decomposition. The results show that for PC1, the AO leading correlation is negative at day −4; at day 0, the correlation between AO and PC2 reaches the positive maximum. This is consistent with the conclusions of the previous phase transmission, but it indicates the intraseasonal relationship between the AO anomalies and the temperature of the EAWM.

In general, a positive AO anomaly corresponds to cold temperatures at high latitudes and warm temperatures at middle latitudes. At the intraseasonal scale, we regress the air temperature at 2 m onto the AO index, and the results are shown in Fig. 8. A warm center is located in Lake Baikal (Fig. 8a) when the AO undergoes a positive anomaly, corresponding to the negative correlation between the AO index and PC1 (Fig. 7), and in the middle troposphere (500 hPa, Fig. 8b), the geopotential height has the pattern of a '+' '−' '+' Rossby wave train in the middle latitude regions. Therefore, we conclude that the AO anomaly influences the air temperature of the EAWM by stimulating the mid-latitude Rossby wave.

5. The influences of the plateau

Terrain has an important influence on the eastern Asian winter climate. The intraseasonal temperature mode has a center in downstream from the Tibetan Plateau (Figs 4b and 6b). RegCM4 is used to simulate the climate from 1999 to 2008. In

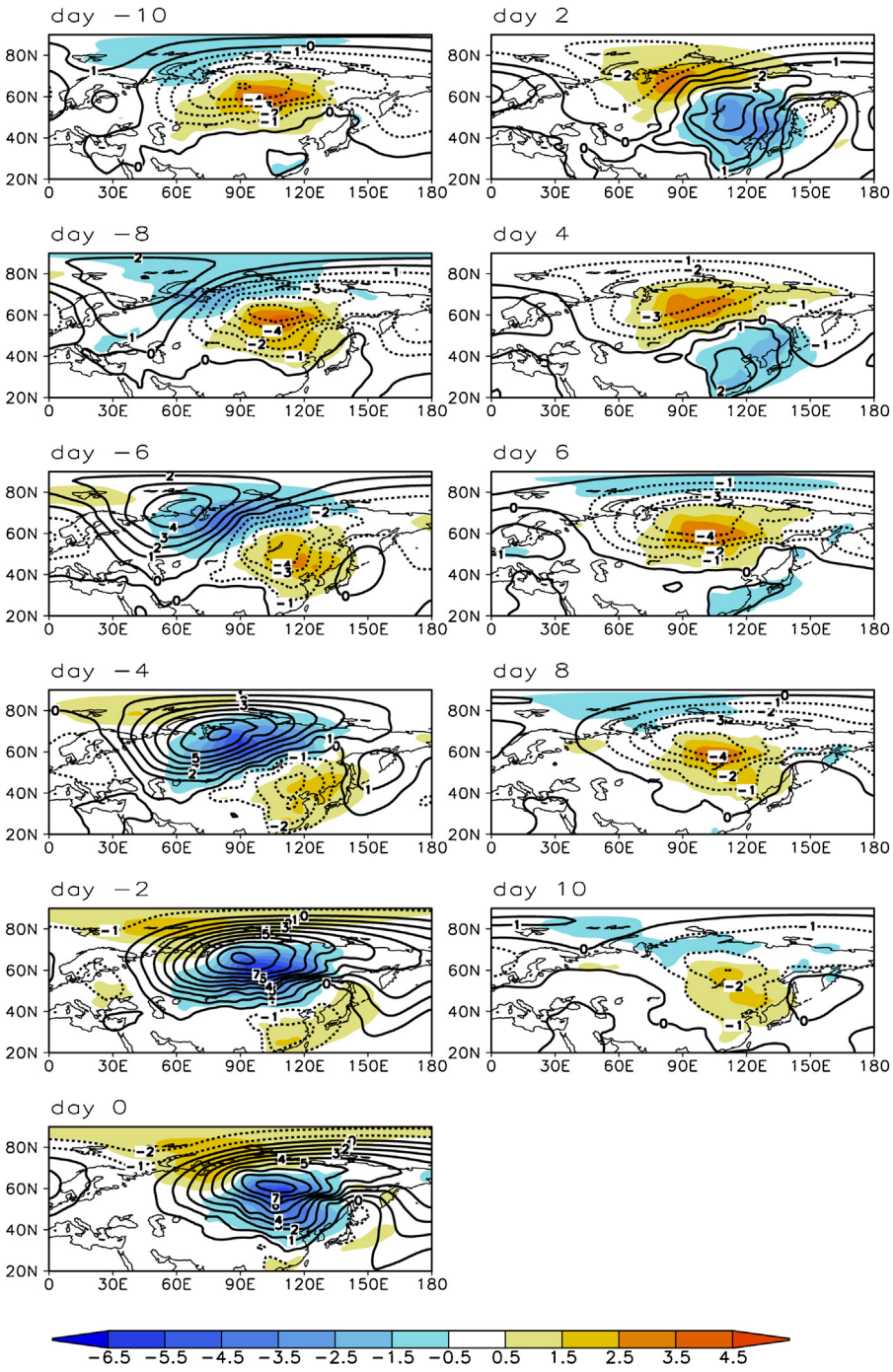

Fig. 5. Evolution of the composite 10–30 day filtered surface air temperature anomalies (color shaded, unit: K) and SLP (contour, unit: hPa) from day −10 to 10, with an interval of 2 days. (For interpretation of the references to colour in this figure legend, the reader is referred to the web version of this article.)

the 9 winters, the surface air temperature of the EAWM in CTR (Fig. 9a) is similar to that of the observations (Fig. 1), and because of the high altitude, the surface air temperature is low in the Tibetan Plateau and the Mongolian Plateau. In the NOP sensitivity experiment, because the land is uniform, it is warm at low latitude and in the ocean and cold at high latitudes (Fig. 9b).

On the intraseasonal time scale, the first EOF modes of the intraseasonal surface air temperature simulated by the different experiments are shown in Fig. 10. The simulated air temperatures are first filtered by a 10–30 window, and then the EOF decomposition method is used to analyze the temperature distribution and the evolution. The variance contribution of the EOF1 of CTR is 15.4% and is 19.3% for the NOP run. The EOF1 of CTR run describes the intraseasonal temperature center

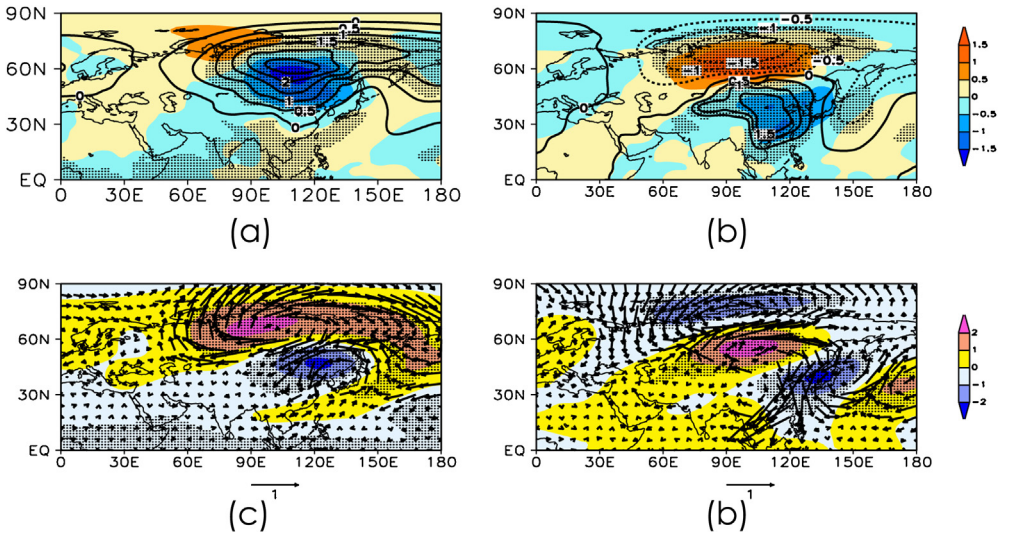

Fig. 6. The regression to PC1 (a, c) and PC2 (b, d) on the intraseasonal time scale. a and b are for the temperature at 2 m (color shaded, unit: K) and sea level pressure (contour, unit: hPa); c and d are for the geopotential height at 500 hPa (color shaded, unit: dagpm) and the wind at 850 hPa (vector, unit: m s^{-1}). The black dotted region denotes the 0.001 significance level. (For interpretation of the references to colour in this figure legend, the reader is referred to the web version of this article.)

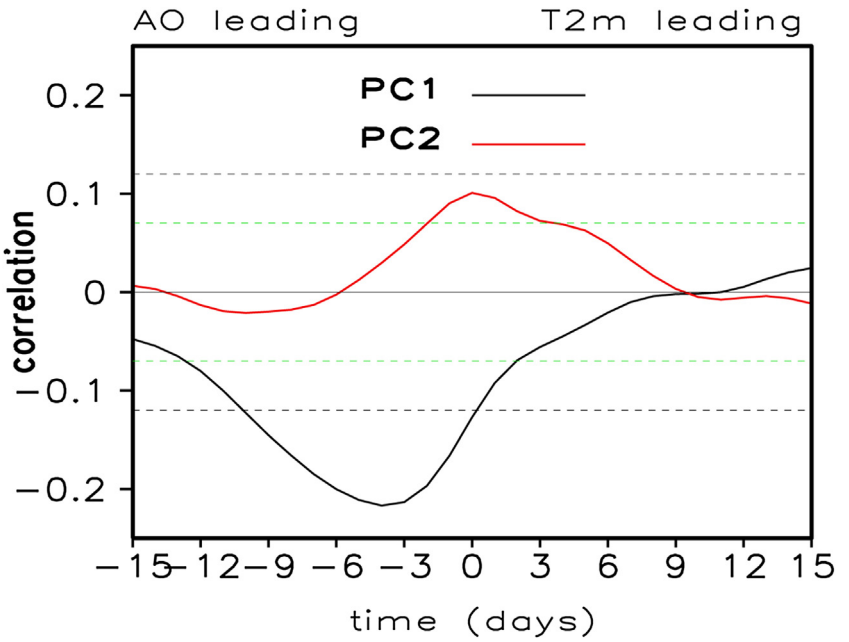

Fig. 7. The lead-lag correlations between the AO index and PC1 (black) and PC2 (red) on the intraseasonal scale. The black dashed lines denote the 0.001 significance level, and the blue dashed lines denote the 0.05 significance level. (For interpretation of the references to colour in this figure legend, the reader is referred to the web version of this article.)

downstream from the Tibetan Plateau (Fig. 10a), and the pattern is consistent with the EOF2 of the ERA-interim data (Fig. 4b). After the terrain has been removed, the 10–30-day filtered surface air temperature mode (Fig. 10b) is very different from that of the observations, and the mode has an antiphase between Lake Balkhash and China, which is obviously different from the antiphase between Lake Baikal and South China in CTR.

Based on the PC1 of the intraseasonal surface air temperature (time series of the EOF1), there are 33 ISO events in CTR run and 29 ISO events in NOP run. The frequency in CTR (3.7 per year) is consistent with that in the observations (ERA-interim data, 3.8 per year). The intraseasonal surface air temperature and SLP composition results from day −10 to day 0 are shown in Fig. 11. Although the frequency in the NOP run is less than that in CTR run, the intensity in NOP run (right side) is much stronger than that in the CTR run (left side). In addition, the paths of the low-frequency cyclone and the anticyclone are different between CTR and NOP. At day 0, the low-frequency anticyclone controls South China, and it is cold in South China

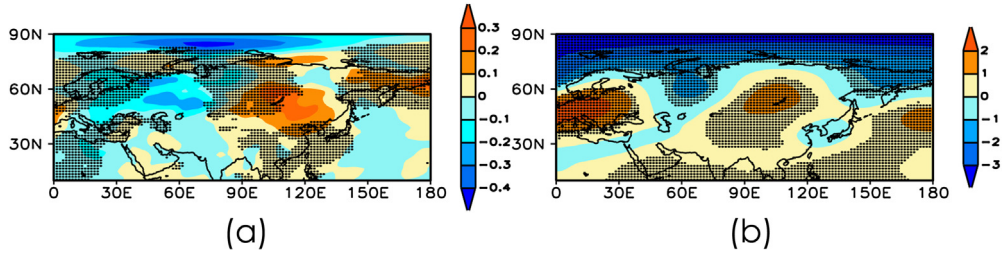

Fig. 8. The regression to the 10–30-day filtered AO index, a: the air temperature at 2 m (unit, K), and b: the geopotential height at 500 hPa (unit: dagpm). The black dotted region denotes the 0.05 significance level.

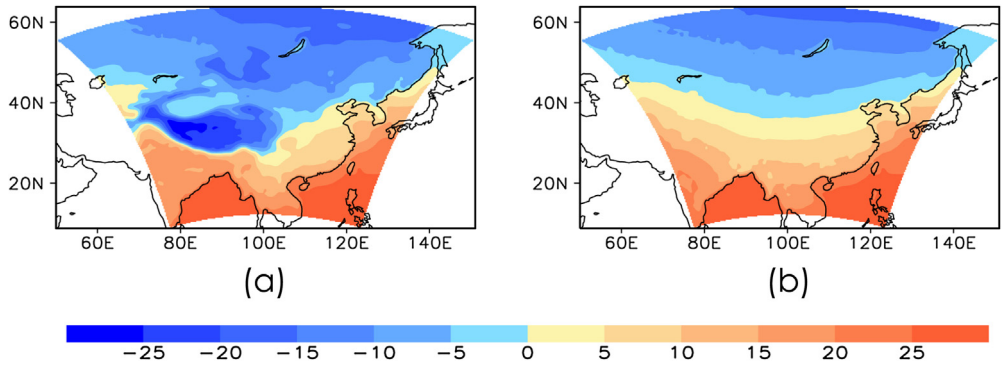

Fig. 9. The winter average (from 1999/2000 to 2007/2008) surface air temperature. (a): CTR; (b): NOP. Unit: ◦C.

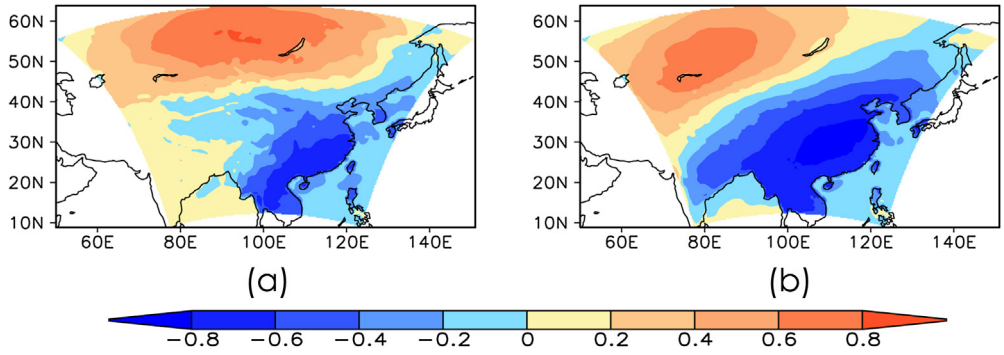

Fig. 10. The first EOF mode of the 10–30-day filtered surface air temperature in winter. (a): CTR; (b): NOP.

and warm in Lake Baikal in CTR. However, once the plateau has been removed, the center of the low-frequency anticyclone is located in the region between 30 and 40◦N. The distribution of the intraseasonal temperature and the SLP shows an antiphase between Lake Baikal and South China in CTR, and the strength of the low frequency cyclone is weaker than that of the anticyclone in eastern Asia in different phases. For the homogeneous underlying surface, the strength of the low-frequency anticyclone and cyclone is the same in eastern Asia in different phases. The low-frequency anticyclone moves southward to South China in CTR and the ERA-interim data, but propagates eastward in NOP.

The movement of the surface cyclone and anticyclone system is generally affected by the steering flow, such as the basic airstream in the middle troposphere. Fig. 12 shows the winter average wind and the geopotential height at 500 hPa. RegCM4 can describe the basic flow in the middle troposphere (Fig. 12a,c). There are some differences between CTR and NOP run. When the plateau is removed, an anomalous cyclone appears in the simulated region at 500 hPa (Fig. 12c). The position with the maximum value of the 10–30-day filtered SLP is defined as the center of the low-frequency anticyclone. From day −10 to day 10, the centers of the intraseasonal anticyclone are signed and connected to be the path of the anticyclone. For the observation data (Fig. 12c, the red line), the intraseasonal anticyclone moves from the Arctic Ocean to Lake Baikal, which is consistent with the steering flow; when it arrives at Lake Baikal, it then propagates southward, although the basic flow is northwest, mainly west. The center of the low-frequency anticyclone can reach South China (approximately 20◦N) and eventually moves to the northwestern Pacific. In CTR (Fig. 12c, green line), the low frequency anticyclone moves southward from Lake Baikal to South China and finally reaches the northwestern Pacific. The path of the intraseasonal anticyclone in CTR

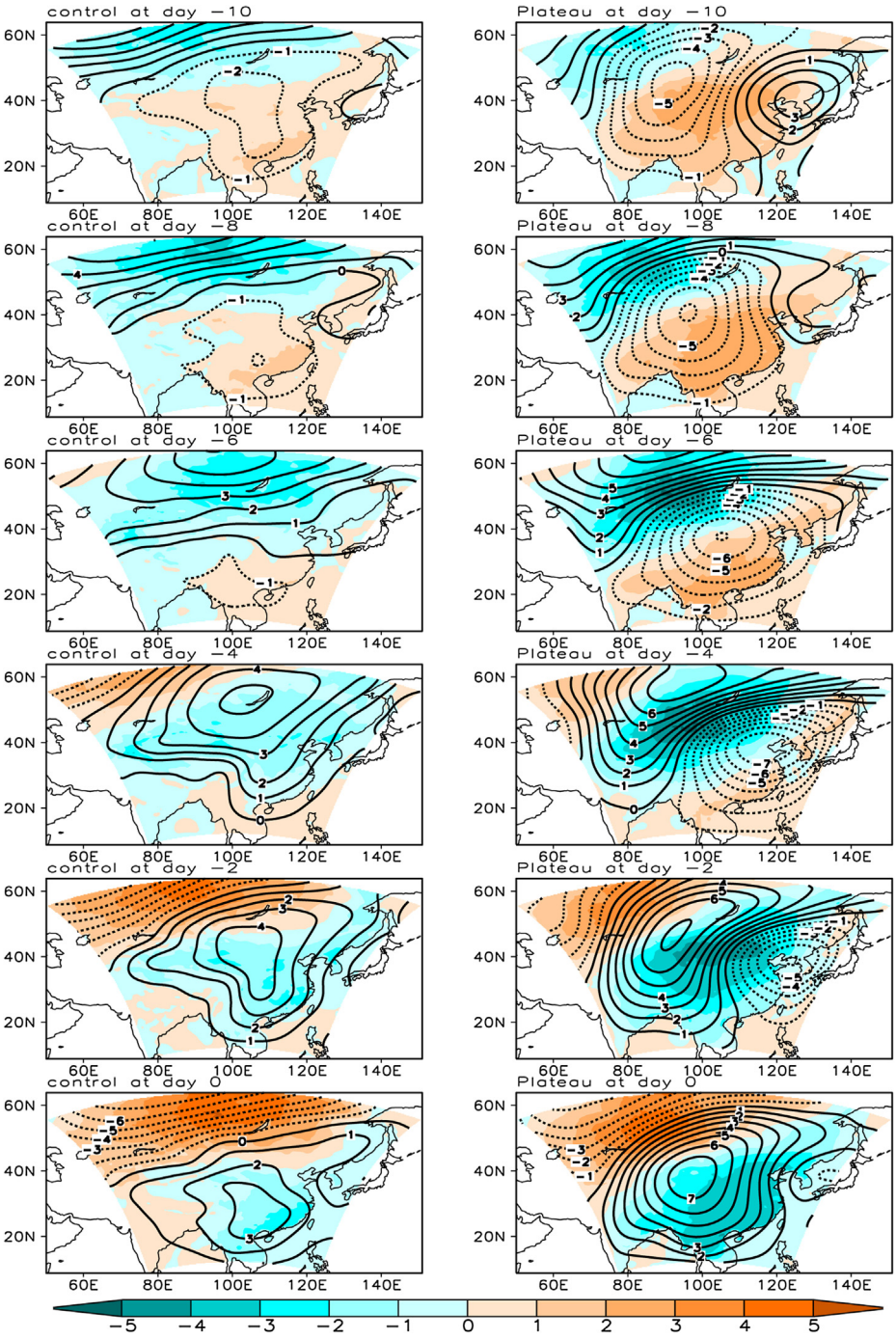

Fig. 11. Evolution of the composite 10–30 day filtered air temperature anomalies (color shaded, unit: K) and the SLP (contour, unit: hPa) from day −10 to 0, with an interval of 2 days. The left side is the result of CTR, and the right side is the result of NOP. (For interpretation of the references to colour in this figure legend, the reader is referred to the web version of this article.)

declines toward the west. In NOP run (Fig. 12c, blue line), although the low-frequency anticyclone moves southward from Lake Baikal, when the center of the anticyclone arrives at 37°N, it moves eastward. Therefore, the plateau has an important influence on the intraseasonal SLP and surface air temperature. The east wind anomaly in Lake Baikal shifts the path to the west in NOP run, and the south wind anomaly prevents the intraseasonal anticyclone from moving southward. If there is no plateau in western China and its upstream region, the intraseasonal anticyclone cannot reach South China.

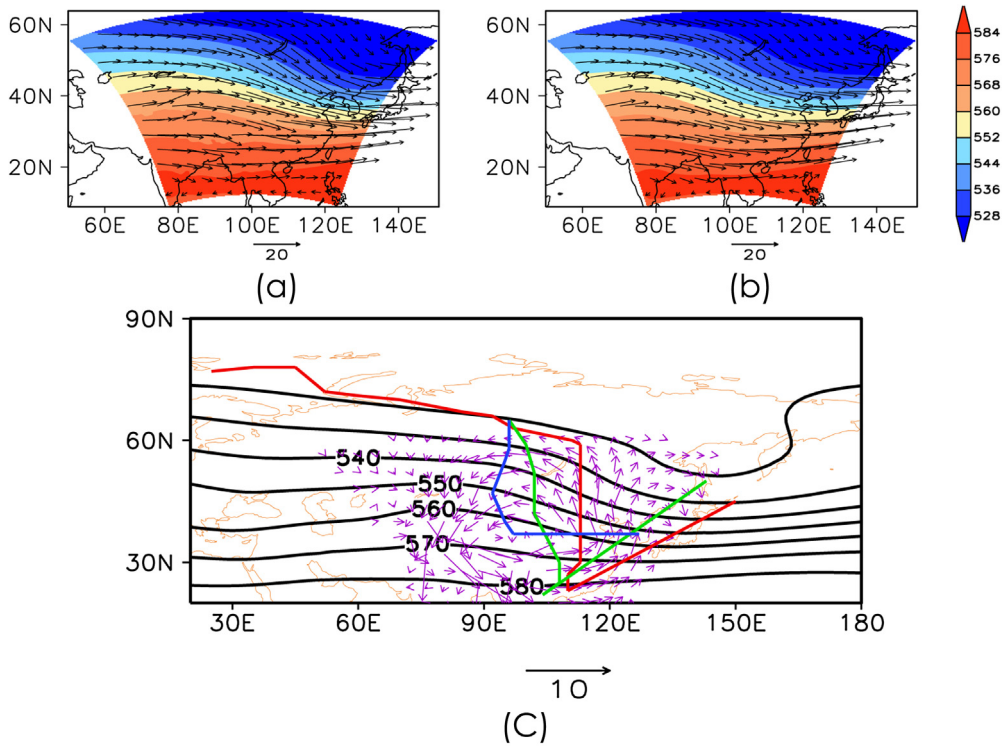

Fig. 12. The simulated winter average geopotential height (shaded, unit: dagpm) and the wind (vector, unit: m s^{-1}) at 500 hPa; (a) CTR and (b) NOP. In (c), the contoured lines are the winter average geopotential height at 500 hPa of ERA-Interim; the vector represents the difference between the winter average wind of NOP and that of CTR; the red, green and blue lines indicate the intraseasonal anticyclone (surface) paths in the ERA-interim data, CTR and NOP, respectively. (For interpretation of the references to colour in this figure legend, the reader is referred to the web version of this article.)

6. Conclusions and discussions

The East Asian winter monsoon is very strong, but research on the intraseasonal oscillation of the EAWM is rare. The present paper uses the ERA-interim 6 h reanalysis data to study the ISO of the air temperature at 2 m and the relationship between the air temperature and the circulation in the Northern Hemisphere.

There is a northerly wind at the surface between the Mongolian high and the Aleutian low, which is the East Asian winter monsoon region. From the winter of 1979/1980 to that of 2012/2013, the first EOF mode of the daily air temperature at 2 m has its center in Lake Baikal, and the second EOF mode has an antiphase between Lake Baikal and China on land. Both temperature modes have a dominant period of 10–30 days. On an intraseasonal time scale, the distribution of the EOF decomposition is similar to that of the raw data. The first EOF mode leads the second mode by 4 days. The intraseasonal cold air spreads from the high latitude of Novaya Zemlya to Lake Baikal and then to China. Over the ocean, the strength of the air temperature ISO is weaker than that over land. The evolution of the intraseasonal temperature and SLP indicates the propagation path and the two temperature modes.

When it is cold in Lake Baikal (negative center), an anomalous low-frequency high controls the north of Eurasia, corresponding to warm temperatures at high latitudes and cold temperatures at middle latitudes. For the EOF2 of the 10–30-day filtered temperature, a low-frequency cyclone controls Lake Baikal, and the low-frequency high moves to China. The low-frequency high at the surface appears between the positive and negative centers of the geopotential height at 500 hPa, and the intraseasonal cold air is in front of the low-frequency anticyclone.

The AO anomaly is closely related to the temperature of the EAWM on the intraseasonal scale. The intraseasonal positive (negative) AO anomaly corresponds to warm (cold) temperature in Lake Baikal, especially when the AO leads the temperature by 4 days. The intraseasonal AO anomaly can stimulate the Rossby wave in the mid-latitude region and affects the surface temperature of the EAWM.

The ladder terrain of eastern Asia has an important influence on the surface air temperature ISO. The sensitivity experiments indicate that the plateau in western China and its upstream regions changes the average temperature distribution and the basic circulation and controls the propagation of the low-frequency anticyclone by changing the steering flow. The plateau causes the low-frequency anticyclone and the movement of cold air to South China.

However, this paper does not explain the mechanism of the Arctic Oscillation's influence on the air temperature ISO in detail, and we think that the mechanism is very complex and worthy of further research. In addition, the general circulation model (GCM) is insufficient to simulate the ISO at middle and high latitudes (Park et al., 2010), so the model used in this

study is a regional model. We set the altitude to 0 in the plateau run, but the driven fields of the lateral boundary include some signals of the terrain. In future study, both the dynamic and the thermal influence of the plateau on the intraseasonal temperature should be included.

Acknowledgments

This work was jointly supported by the Scientific Research Foundation for Returned Overseas Chinese Scholars, State Education Ministry 2015s009, the National Basic Research Program of China under grants 2015CB453201, BK20150062, the program of KLME1308, and the Priority Academic Program Development of Jiangsu Higher Education Institutions (PAPD).

References

Anderson, J.R., Rosen, R.D., 1983. The latitude-height structure of 40–50 day variations in atmospheric angular momentum. J. Atmos. Sci. 40, 1584–1591.
Chatterjee, P., Goswami, B.N., 2004. Structure: genesis and scale selection of the tropical quasi-biweekly mode. Q. J. R. Meteorol. Soc. 130, 1171–1194.
Dee, D.P., Uppala, S.M., Simmons, A.J., et al., 2011. The ERA-Interim reanalysis: configuration and performance of the data assimilation system. Q. J. R. Meteorol. Soc. 137, 553–597.
Dickinson, R.E., Errico, R.M., Giorgi, F., Bates, G.T., 1989. Aregional climate model for the western United States. Clim. Change 15, 383–422.
Gao, X.J., Wang, M.L., Filippo, G., 2013. Climate change over China in the 21 st century as simulated by BCC_CSM1.1-RegCM4.0. Atmos. Ocean. Sci. Lett. 5, 381–386.
Ghil, M., Mo, K., 1991. Intraseasonal oscillations in the global atmosphere: part I: northern hemisphere and tropics. J. Atmos. Sci. 48, 752–779.
Giorgi, F., Mearns, L.O., 1999. Introduction to special section: regional climate modeling revisited. J. Geophys. Res. 104, 6335–6352.
Hamming, R.W., 1977. Digital Filters. Prentice-Hall, Englewood Cliffs, N.J.
Hendon, H.H., Salby, M.L., 1994. The life cycle of the Madden–Julian oscillation. J. Atmos. Sci. 51, 2225–2237.
Higgins, R.W., Leetmaa, A., Xue, Y., Barnston, A., 2000. Dominant factors influencing the seasonal predictability of U.S. precipitation and surface air temperature. J. Clim. 13, 3994–4017.
Higgins, R.W., Leetmaa, A., Kousky, V.E., 2002. Relationships between climate variability and winter temperature extremes in the United States. J. Clim. 15, 1555–1572.
Hsu, P.C., Li, T., 2012. Role of the boundary layer moisture asymmetry in causing the eastward propagation of the Madden–Julian oscillation. J. Clim. 25, 4914–4931.
Hsu, P.C., Lee, J.Y., Ha, K.J., 2015. Influence of boreal summer intraseasonal oscillation on rainfall extremes in southern China. Int. J. Climatol., http://dx.doi.org/10.1002/joc.4433.
Jiang, X., Li, T., Wang, B., 2004. Structures and mechanisms of the northward propagating boreal summer intraseasonal oscillation. J. Clim. 17, 1022–1039.
Kiladis, G.N., Wheeler, M., 1995. Horizontal and vertical structure of observed tropospheric equatorial Rossby waves. J. Geophys. Res. 100, 22981–22982.
Knutson, T.R., Weickmann, K.M., 1987. 30-60 day atmospheric oscillations: composite life cycles of convection and circulation anomalies. Mon. Weather Rev. 115, 1407–1436.
Krishnamurti, T., Gadgil, S., 1985. On the structure of the 30 to 50 day mode over the globe during FGGE. Tellus 37A, 336–360.
Li, T., 2014. Recent advance in understanding the dynamics of the Madden–Julian oscillation. Acta Meteorol. Sinica 28, 1–33.
Lin, A., Li, T., 2008. Energy spectrum characteristics of boreal summer intraseasonal oscillations: climatology and variations during the ENSO developing and decaying Phases. J. Clim. 21, 6304–6320.
Ma, N., Li, Y., Ju, J., 2011. Intraseasonal oscillation characteristics of extreme cold: snowy and freezing rainy weather in Southern China in early 2008. Plateau Meteor 30, 318–327.
Madden, R.A., Julian, P.R., 1971. Detection of a 40–50-day oscillation in the zonal wind in the tropical Pacific. J. Atmos. Sci. 28, 702–708.
Madden, R.A., Julian, P.R., 1972. Description of global-scale circulation cells in the tropics with a 40–50 day period. J. Atmos. Sci. 29, 1109–1123.
Madden, R.A., Julian, P.R., 1994. Observations of the 40–50 day tropical oscillation-a review. Mon. Weather Rev. 122, 814–837.
Maloney, E.D., 2009. The moist static energy budget of a composite tropical intraseasonal oscillation in a climate model. J. Clim. 22, 711–729.
Mao, J., Chan, J., 2005. Intraseasonal variability of the south China sea summer monsoon. J. Clim. 18, 2388–2402.
Pal, J.S., Giorgi, F., Bi, X., Elguindi, N., et al., 2007. Regional climate modeling for the developing world: the ICTP RegCM3 and RegCNET. Bull. Am. Meteorol. Soc. 88, 1395–1409.
Park, S., Hong, S.Y., Byun, Y., 2010. Precipitation in boreal summer simulated by a GCM with two convective parameterization schemes: implications of the intraseasonal oscillation for dynamic seasonal prediction. J. Clim. 23, 2801–2816.
Shao, X., Zhang, Z.Q., Tao, L., 2011. Influence analysis of quasi-biweekly oscillation during the low temperature: rain and snow weather in South China in 2007/2008 winter. Meteorol. Enviro. Sci. 34, 1–6.
Slingo, J.M., Rowell, D.P., Sperber, K.R., Nortley, F., 1999. On the predictability of the interannual behaviour of the Madden–Julian Oscillation and its relationship with El Niño. Q. J. R. Meteorol. Soc. 125, 583–609.
Sperber, K.R., 2003. Propagation and the vertical structure of the Madden–Julian oscillation. Mon. Weather Rev. 131, 3018–3303.
Tang, W.Y., Guan, Z.Y., 2015. ENSO-independent contemporaneous variations of anomalous circulations in the Northern and Southern Hemispheres: the polar-tropical seesaw mode. J. Meteorolog. Res. 29 (6), 917–934.
Thompson, D.W.J., Wallace, J.M., 1998. The Arctic Oscillation signature in the wintertime geopotential height and temperature fields. Geophys. Res. Lett. 25, 1297–1300.
Wang, L., Li, T., Zhou, T., 2012. Intraseasonal SST variability and air sea interaction over the Kuroshio Extension region during boreal summer. J. Clim. 25, 1619–1634.
Wang, L., Li, T., Zhou, T., Rong, X., 2013. Origin of the intraseasonal variability over the North Pacific in boreal summer. J. Clim. 26, 1211–1229.
Yang, S., Li, T., 2016a. Intraseasonal variability of air temperature over the mid-high latitude Eurasia in boreal winter. Clim. Dyn., http://dx.doi.org/10.1007/s00382-015-2956-8.
Yang, S., Li, T., 2016b. Zonal shift of the South Asian High on the subseasonal time-scale and its relation to the summer rainfall anomaly in China. Q. J. R. Meteorol. Soc., http://dx.doi.org/10.1002/qj.2826.
Yang, J., Wang, B., Wang, B., Bao, Q., 2010. Biweekly and 21–30-dayvariations of the subtropical summer monsoon rainfall over the Lower Reach of the Yangtze River Basin. J. Clim. 23, 1146–1159.
Zhou, S., Miller, A.J., Wang, J., Angell, K.E., 2001. Trends of NAO and AO and their associations with stratospheric processes. Geophys. Res. Lett. 28, 4107–4110.
Zhu, Z., Li, T., 2016. The statistical extended-range (10–30-day) forecast of summer rainfall anomalies over the entire China. Clim. Dyn., http://dx.doi.org/10.1007/s00382-016-3070-2.